Parallel Adaptive Simulation of Detonation Waves Using a Weighted Essentially Non-Oscillatory Scheme

Sean McMahon

A thesis submitted in partial fulfillment of the
requirements for the degree of

Master of Science

University of Washington

2014

Reading Committee:

Antonino Ferrante, Chair

Mitsuru Kurosaka

Program Authorized to Offer Degree:
Master of Science in Aeronautics and Astronautics

0

University of Washington

Abstract

Parallel Adaptive Simulation of Detonation Waves Using a Weighted Essentially Non-Oscillatory Scheme

Sean McMahon

Chair of the Supervisory Committee:
Professor Antonino Ferrante
Williams E. Boeing Department of Aeronautics and Astronautics

The purpose of this thesis was to develop a code that could be used to develop a better understanding of the physics of detonation waves. First, a detonation was simulated in one dimension using ZND theory. Then, using the 1D solution as an initial condition, a detonation was simulated in two dimensions using a weighted essentially non-oscillatory scheme on an adaptive mesh with the smallest lengthscales being equal to 2-3 flamelet lengths. The code development in linking Chemkin for chemical kinetics to the adaptive mesh refinement flow solver was completed. The detonation evolved in a way that, qualitatively, matched the experimental observations, however, the simulation was unable to progress past the formation of the triple point.

TABLE OF CONTENTS

Page

LIST OF FIGURES

ACKNOWLEDGMENTS

I would like to express my great appreciation to the William E. Boeing department of Aeronautics and Astronautics at the University of Washington for accepting me to their program, Profesors Antonino Ferrante and Mitsuru Kurosaka for advising me in my research, the Royal Research Fund for funding my research and the eScience Institute and UW-IT for maintaining the Hyak Supercomputer that this research was conducted on.

Chapter 1

INTRODUCTION

A detonation occurs when a combustion wave, a moving chemically reacting front, becomes supersonic. This phenomenon may occur in nature, through engineering to serve a particular purpose, or by accident.

The physical phenomenon of detonation is exploited by engineers for the purpose of demolishing old buildings efficiently, mining and for defense. These purposes require the extremely high, efficiently produced, energy that comes from a detonation. However, given the applications, an exact quantification is hardly necessary to exploit the phenomenon.

A new application of this phenomenon that has gained interest in recent years is the detonation engine. This device uses the efficient, high energy release process of detonation to accelerate gases and produce thrust for aircraft. The difference between the applications of detonation to propulsion and demolition is that for propulsive purposes the detonations have to be controlled. In order to do this, it is necessary to obtain a deeper understanding of the physics of this phenomenon that was not necessary for the case of detonation for the purpose of demolition. Developing a reliable control strategy for such an engine is not possible if the response to the actuators used to control it is unknown.

Understanding of the detonation phenomenon is limited due to the difficulties in obtaining data from physical experiments. Imaging devices capable of capturing the structure of a detonation wave and the facilities where a detonation wave can be studied are extremely expensive and proliferation of them, as a result, is not high. However, in the absence of these apparatus, computational tools can be utilized to obtain data that would otherwise not be possible.

The purpose of this thesis is to develop computational codes that can be used to understand the physics of detonation waves.

1.1 One Dimensional Detonation Theories

Despite the lack of understanding that exists for the case of two and three dimensional detonation, for the unidirectional case, the physics is well understood and there are comprehensive theories explaining the dynamics of these waves. Although, it is rarely the case that a detonation does not have any transverse disturbances, the values obtained from the idealized case of a one dimensional detonation are useful in the understanding of more complex, multidimensional detonation waves. These have been developed first by Chapman (1889) and Jouguet (1904) and then by Zeldovich (1940), von Neumann (1942) and Döring (1943).

1.1.1 Chapman Jouguet Theory

For given initial and boundary conditions, the possible combustion waves that can occur are given by the solutions to the one dimensional conservation equations across the wave. Here we follow the description by Lee (2008)

$$\rho_0 u_0 = \rho_1 u_1 \tag{1.1}$$

$$p_0 + \rho_0 {u_0}^2 = p_1 \rho_1 {u_1}^2 \tag{1.2}$$

$$h_0 + \frac{u_0^2}{2} = h_1 + \frac{u_1^2}{2} \tag{1.3}$$

where 0 and 1 represent the reactant and product states respectively.

The energy equation can be rewritten more simply by separating the formation and sensible enthalpies. The formation enthalpy is the enthalpy that a substance possesses when created at room temperature. The sensible enthalpy is the difference between the enthalpy at room temperature and at the actual temperature.

$$h_0 + q + \frac{u_0^2}{2} = h_1 + \frac{u_1^2}{2} \tag{1.4}$$

where

$$q = \sum_{i}^{reactants} Y_i h_{f_i}^o - \sum_{j}^{products} Y_j h_{f_j}^o \tag{1.5}$$

From this, the thermodynamic path that the initial state takes to the final state can be determined.

These can be rewritten using thermodynamic relations as the Rayleigh line.

$$y = (1 + \gamma_0 M_0^2) - (\gamma_0 M_0^2)x \tag{1.6}$$

where

$$x = \frac{\rho_0}{\rho_1} \tag{1.7}$$

and

$$y = \frac{p_1}{p_0} \tag{1.8}$$

Using thermodynamic relations and the energy conservation equation, the Hugoniot curve can be shown as follows.

$$(y + \alpha)(x - \alpha) = \beta \tag{1.9}$$

Where

$$\alpha = \frac{\gamma_1 - 1}{\gamma_1 + 1} \tag{1.10}$$

$$\beta = \alpha \left(\frac{\gamma_0 + 1}{\gamma_0 - 1} - \alpha + 2q' \right) \tag{1.11}$$

The intersection of these two lines must necessarily be the velocity of the detonation wave. However, as is shown in Fig. 1.1, according to the conservation laws across the $1D$ detonation, there are two possible propogation velocities.

Chapman's hypothesis, given that only one solution was obtained for any given mixture was that the minimum velocity detonation, which had a unique solution, must be the correct

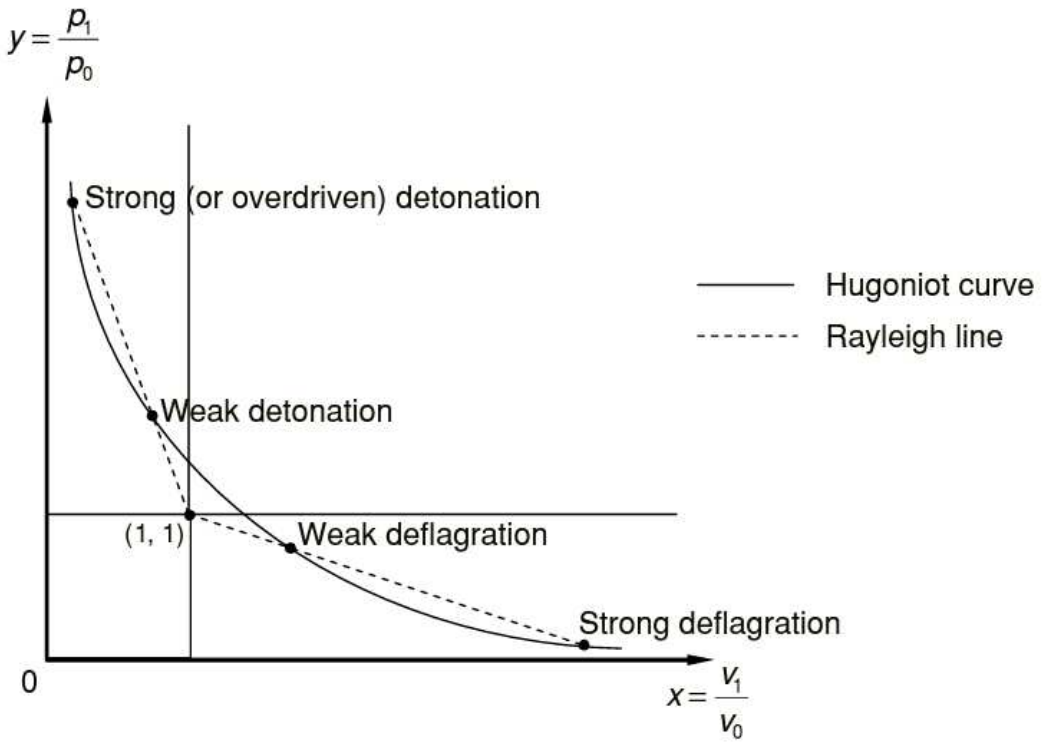

Figure 1.1: An illustration of the Rankine line and Hugoniot curve intersections (Lee (2008)).

one. Jouguet's theory was that the flow must be sonic downstream the detonation. He also observed that this corresponded with the minimum entropy solution. These hypotheses lead to the same general conclusion.

It has since been found that the reason that detonation tend to this propagation velocity is that detonations elsewhere on the Hugoniot curve are inherently unstable. A detonation on the Hugoniot curve with a higher velocity than the CJ velocity is unstable because, for this kind of detonation, the flow behind it is subsonic, allowing expansion waves to enter the reaction zone and attenuate the reactions. The strong detonation solution can, however, exist for the case of piston driven detonation.

In the reaction zone of a detonation wave, there are infinitely many possible Hugeonoit curves depending on when the initial state is defined. If none of these curves intersect, then weak detonations cannot occur. However, if the curves do intersect, then weak detonations are possible. Reactants that have an overshoot in temperature due to a fast exothermic reaction followed by a slower endothermic reaction do result in weak detonations. $H_2 + Cl_2$ detonation is an example of this (Ratner & Zeldovich (1941)). None of the detonations analyzed in this study have this property. Most detonations that occur naturally or are engineered do not have this property.

1.1.2 ZND Theory

The Chapman-Jouguet theory for detonation waves explains the downstream states and velocity of the detonation wave well. However, no reaction is infinitely fast and any theory that assumes this is, as a result, incomplete.

The ZND theory decomposes the detonation wave into four sections, as shown by Fig. 1.2.

The first section is the unreacted state. The detonation has no effect on it given the fact that information propagates through a fluid at the speed of sound and the detonation wave, by definition, must be traveling faster than this.

The second section of the figure represents the induction zone. The thermodynamic properties in this zone are the same as those if a non reacting shock had compressed the

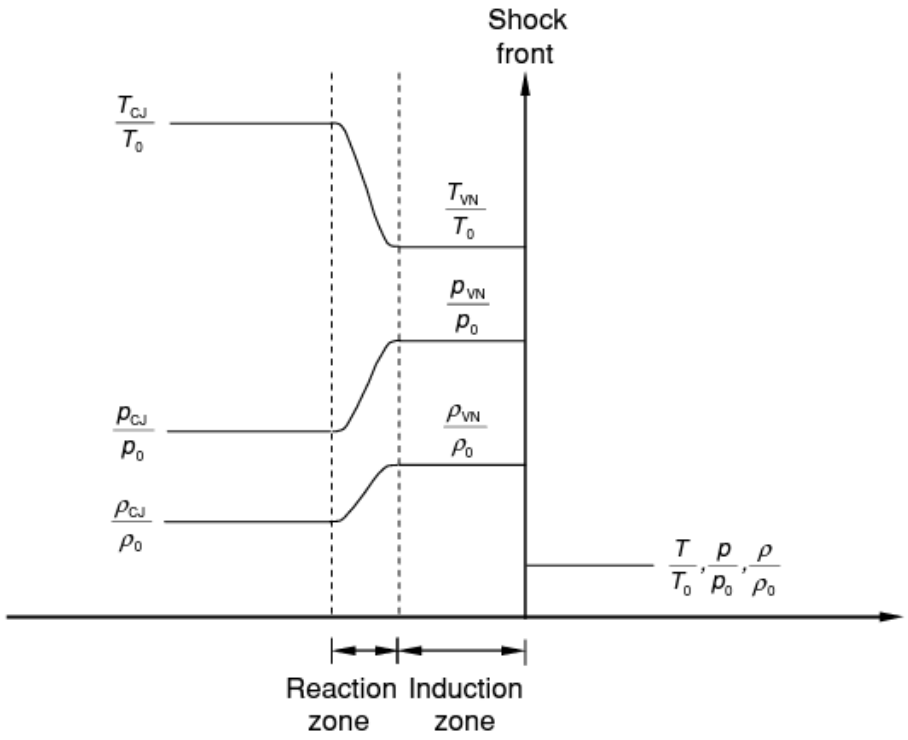

Figure 1.2: An illustration of the four sections of a detonation (Lee (2008)).

initial gas. The chemical composition does not change in this zone.

Because the one dimensional detonation structure is temporally constant for most practical detonations, it is convenient to analyze the detonation structure in a frame of reference that is following the shockwave for the calculate of the shock jump properties. The translation is shown in Eq. 1.12 and 1.13.

$$w_1 = U_s - u_1 \tag{1.12}$$

$$w_2 = U_s - u_2 \tag{1.13}$$

This is illustrated in Fig 1.3.

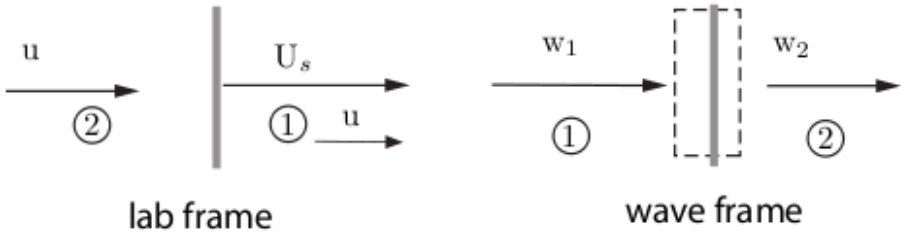

Figure 1.3: An illustration of a stationary reference frame following a detonation wave (Kao & Shepherd (2008)).

In the frame of reference, the non reacting conservation laws can be written as follows.

$$\rho_1 w_1 = \rho_2 w_2 \tag{1.14}$$

$$p_1 + \rho_1 w_1^2 = p_2 + \rho_2 w_2^2 \tag{1.15}$$

$$h_1 + \frac{w_1^2}{2} = h_2 + \frac{w_2^2}{2} \tag{1.16}$$

In the third section, the reactions progress, the VN thermodynamic properties change to the CJ thermodynamics properties and the initial chemical composition transitions to the final chemical composition. This change can be predicted using a system of differential equations.

A useful parameter in the determination of the reaction zone structure is the thermicity. This quantity measures the rate at which chemical energy is transfered to thermal energy and vice versa. This is shown in Eq. 1.17 below, taken from Kao & Shepherd (2008)

$$\dot{\sigma} = \sum_{S}^{i=1} \sigma_i \frac{DY_i}{Dt} \tag{1.17}$$

$$\sigma_i = -\frac{\alpha_T}{Cp} \frac{\partial h_i}{\partial Y_i}|_{p,T,Y_{k\neq i}} \tag{1.18}$$

$$\alpha_T = -\frac{1}{\rho} \frac{\partial \rho}{\partial T}|_{P,Y_k} \tag{1.19}$$

The differential equations describing the spatial variance in the reaction zone are as follows

$$\frac{d\rho}{dx} = -\frac{\rho}{w} \frac{\dot{\sigma}}{1 - M^2} \tag{1.20}$$

$$\frac{dw}{dx} = \frac{\dot{\sigma}}{1 - M^2} \tag{1.21}$$

$$\frac{dP}{dx} = -\rho w \frac{\dot{\sigma}}{1 - M^2} \tag{1.22}$$

$$w \frac{dY_i}{dx} = \dot{\omega}_i \tag{1.23}$$

The spatial and temporal derivatives can then be expressed as

$$\frac{dx}{dt} = w \tag{1.24}$$

The thermodynamic properties in the final section are those that can be calculated from CJ theory and the chemical composition is that of the completely reacted state.

1.2 Unstable Two Dimensional Detonation Studies

1.2.1 ZND Detonation in Two Dimensions

The physics of unidirectional detonation is very comprehensively explained and the parameters obtained from such calculations are useful in the analysis of real detonations, however, real detonations are hardly ever unidirectional. Small pertubations almost always cause instabilities that are three dimensional. To better understand the phenomenon, an experimental investigation of two dimensional detonation is necessary. In experiments, according to (Bone, Fraser & Wheeler (1935)) $\lambda/n \approx 6$ to 10 where λ is the typical cell spacing to transverse thickness ratio that suppresses one direction's detonation mode and makes the detonation two dimensional.

Experiments that adhere to this criterion show the temporal structure detonation front structure shown in Fig. 1.4.

The triple point has a higher local pressure than any other point in the detonation front. A consequence of this is that the indents in deformable geometries that the detonation wave moves across are greater where the tripe point has been. This allows for the tracking of the location of path of this point in space with soot foils. The structure unveiled by this is illustrated in Fig. 1.5.

An important piece of information that can be viewed from these soot foils is that the tracks formed from the trajectory of the triple point form a cellular pattern and for many combinations of gases and initial conditions these cell spacings are consistent in length. This property of two dimensional detonations allows for the of multi dimensional detonation computational models. It is important to note that not all combinations of gases and initial conditions produce regular cellular patterns.

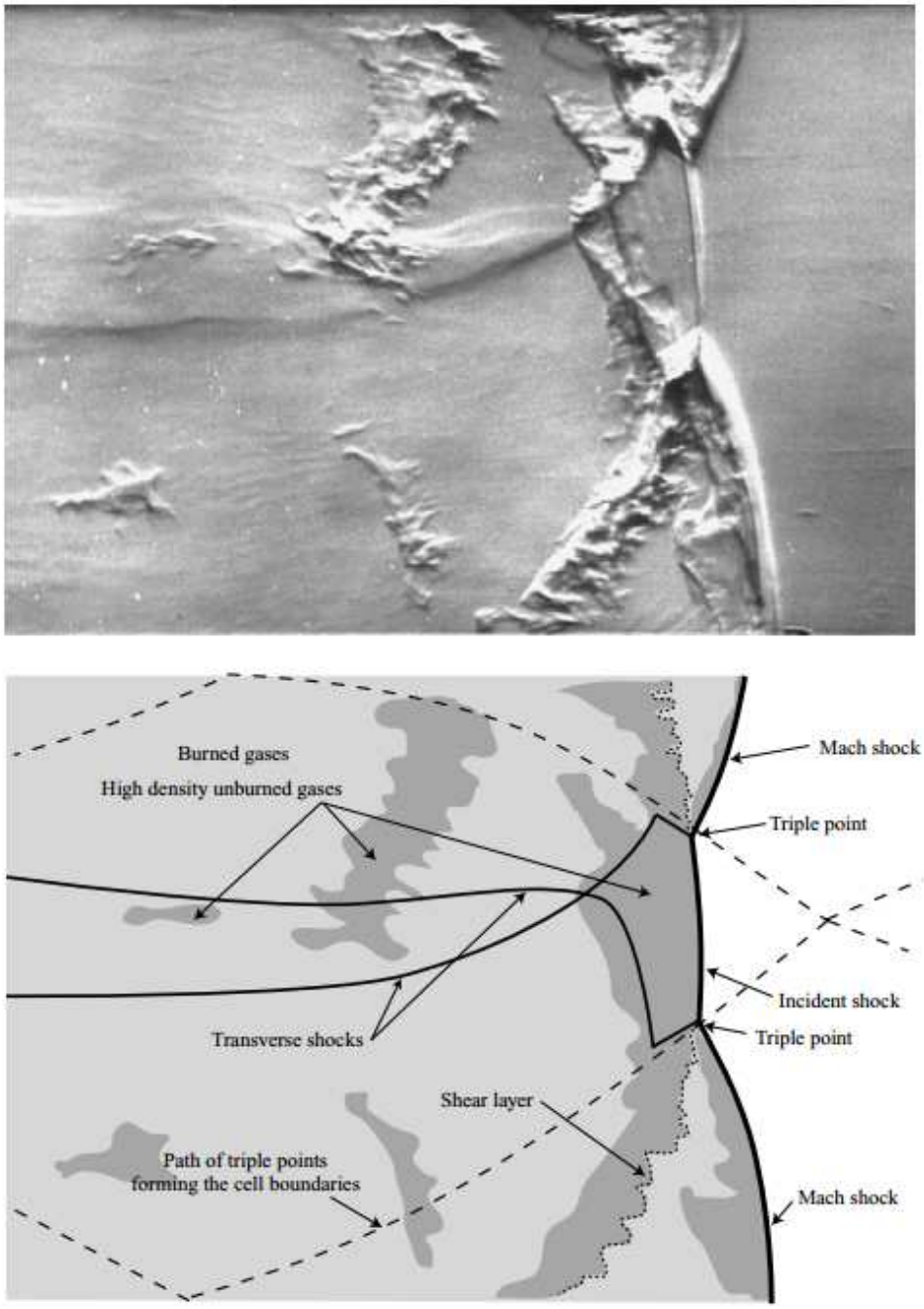

Figure 1.4: An illustration of the two dimensional structure of a detonation wave (Radulescu et al (2007)).

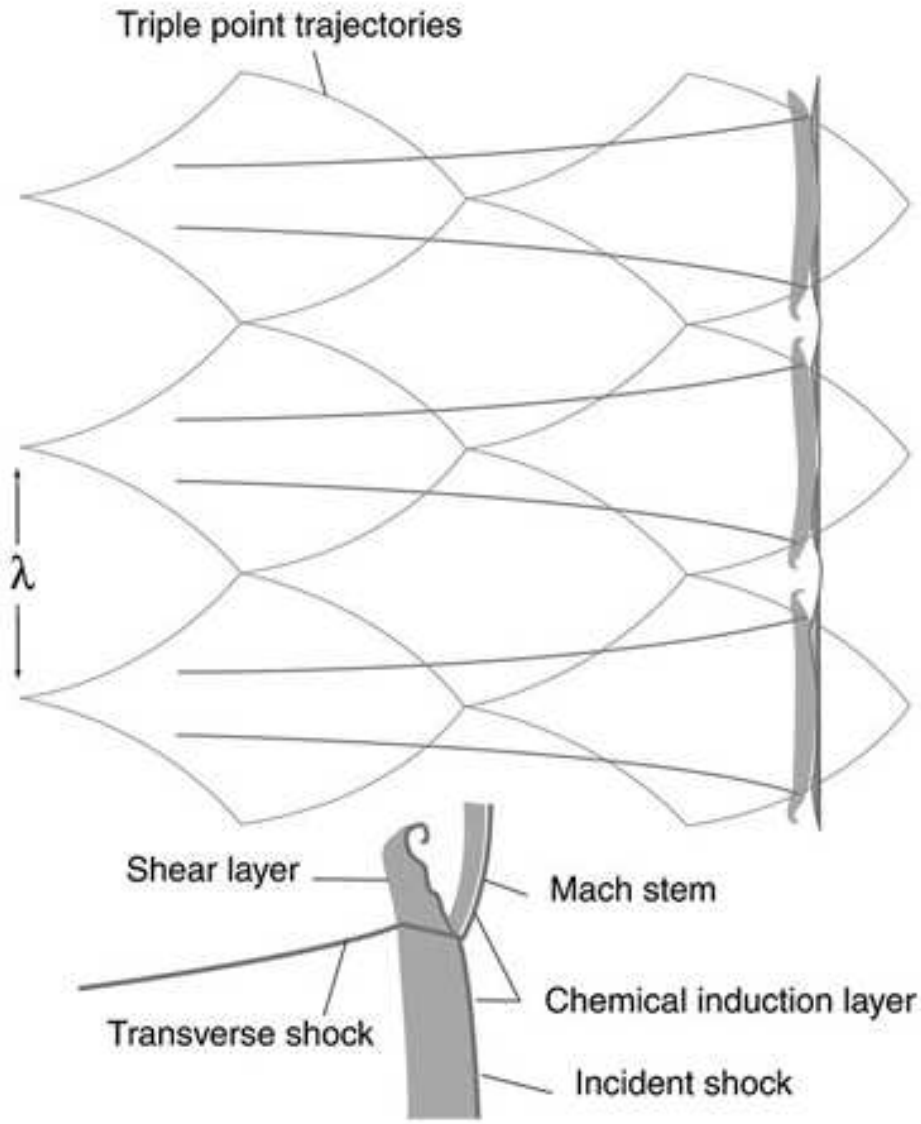

Figure 1.5: An illustration of the time history of the triple point path of a detonation wave (Lee & Radulescu (2005)).

Chapter 2

MATHEMATICAL DESCRIPTION

2.1 Governing Equations

The governing equations for a detonation propagation in premixed gases are the inviscid reactive Euler equations (Williams (1985)), which are as follows.

$$\partial_t \rho_i + \partial_k \left(\rho_i u_k\right) = W_i \dot{\omega}_i, \quad \forall i = 1, ..., S \tag{2.1}$$

$$\partial_t \left(\rho u_j\right) + \partial_k \left(\rho u_j u_k\right) + \partial_j p = 0, \tag{2.2}$$

$$\partial_t \left(\rho E\right) + \partial_k \left[\left(\rho E + p\right) u_k\right] = 0, \tag{2.3}$$

∂_k represents the spatial stream-wise, ∂_x $(k = 1)$, and span-wise, ∂_y $(k = 2)$ directions for $k = 1, 2$, u_k represents the velocity in the k direction and p represents the pressure. W_i represents the molecular mass of the ith species, ρ_i represents the partial density of the ith species and the molar production rate ω_i. The molar production rate is calculated using data from JANAF tables using Chemkin-II (Robert (1989)). The temperature change is calculated during an intermediary step.

2.1.1 The Source Term

The chemical production rates $\dot{\omega}_i$ are derived from a reaction mechanism (Williams (2004)) containing J reactions.

$$\sum_{j=1}^{S} \nu_{ji}^{f} S_i \rightleftharpoons \sum_{j=1}^{S} \nu_{ji}^{r} S_i, \quad j = 1, ...J \tag{2.4}$$

ν_{ji}^{f} and ν_{ji}^{r} are the stoichiometric coefficients of the species for the product and reactant respectively. The molar production rate for the species i is given as follows. The chemical

production rate is calculated using Chemkin-II for a reaction mechanism of J reactions and S species using a two step chemistry model.

$$\dot{\omega}_i = m_i \sum_{j=1}^{J} \left(\nu_{ji}^r - \nu_{ji}^f\right) \left[k_i^f \prod_{l=1}^{S} \left(\frac{\rho_l}{m_l}\right)^{\nu_{jl}^f} - k_j^r \prod_{l=1}^{S} \left(\frac{\rho_l}{m_l}\right)^{\nu_{jl}^r}\right], \quad i = 1, ..., S \tag{2.5}$$

$k_j^f(T)$ and $k_j^r(T)$ represent the forward and backward reaction rates respectively. These are calculated using Arrhenius' Law as follows.

$$k_j^{f/r}(T) = A_j^{f/r} T^{\beta_j^{f/r}} exp(-E_j^{f/r}/\mathcal{R}T) \tag{2.6}$$

2.1.2 Heat Release Effects

The temperature changes when the chemical composition changes in a way that reflects whether the reaction was exothermic or endothermic. According to Deiterding (2002) The temperature can be calculated from a modified form of the definition of enthalpy.

$$\rho h = \rho E + p \tag{2.7}$$

This equation can be broken up into a species specific form to obtain the following.

$$\sum_{i=1}^{S} \rho_i h_i(T) = \rho e + \mathcal{R}T \sum_{i=1}^{S} \frac{\rho_i}{W_i} \tag{2.8}$$

If the terms are rearranged, the following equation is obtained.

$$f(T) = \sum_{i=1}^{S} \rho_i h_i(T) - \rho e - \mathcal{R}T \sum_{i=1}^{S} \frac{\rho_i}{W_i} = 0 \tag{2.9}$$

If the derivative with respect to T is taken of the function f, the following equation is obtained.

$$f'(T) = \sum_{i=1}^{S} \rho_i c_{p_i}(T) - \mathcal{R} \sum_{i=1}^{S} \frac{\rho_i}{W_i} = 0 \tag{2.10}$$

Newton's method can then be used to evaluate the temperature.

$$T_{i+1} = T_i - \frac{f(T)}{f'(T)} \tag{2.11}$$

2.2 Initial Conditions

The initial conditions used the one dimensional solution to the ZND detonation in the streamwise direction and extrapolated it spanwise across the domain.

1. Choose the initial, unreacted, thermodynamic properties and species mass fractions.

2. Use CEA to solve for the VN properties of the detonation wave and obtain the detonation speed D_{CJ}.

3. Solve Eq. 1.20-1.24 to solve for the reaction zone properties. The properties at ∞ are the the CJ properties, so use of the Hugoniot curve and Rayleigh are not necessary.

The result of these $1D$ simulations are shown in Fig. 2.1 and 2.2. These longitudinal solutions will serve as the initial conditions.

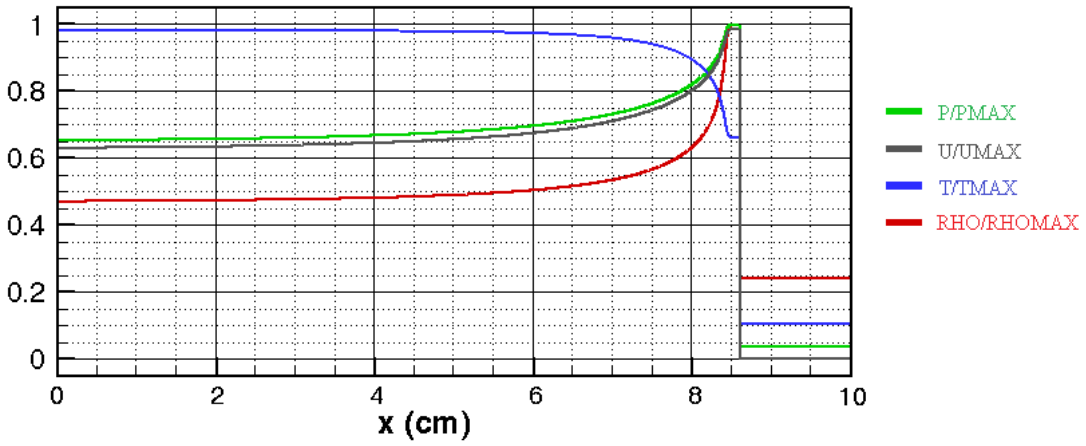

Figure 2.1: A plot of the thermodynamic profile of a one dimensional detonation wave.

To create the two dimensional instabilities that are present in real detonations, it is necessary to include a transverse disturbance. This is done, as was done by Lefebre, Oran &

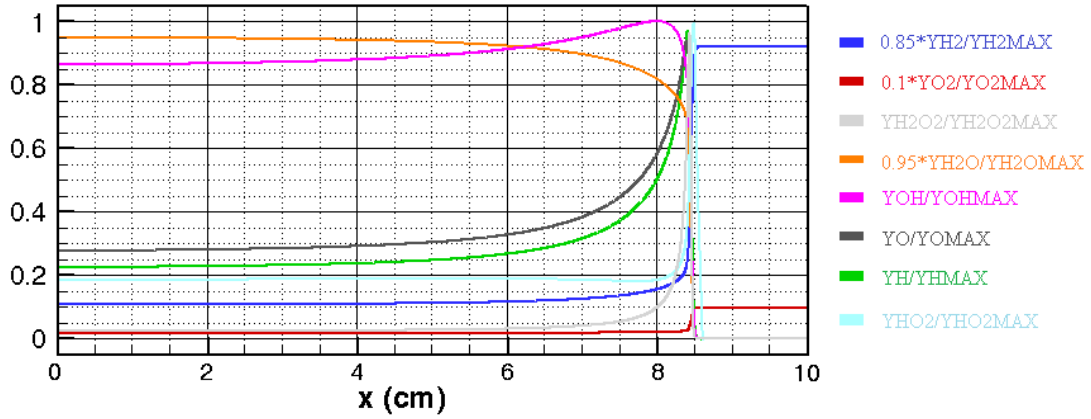

Figure 2.2: A plot of the species profile of the detonation wave.

Kailansanath (1993). by including an unreacted pocket behind the detonation as is shown qualitatively in Fig. 2.3.

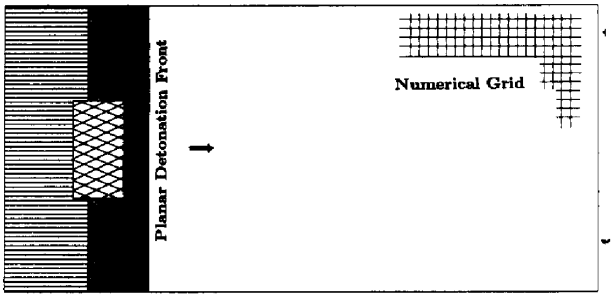

Figure 2.3: An illustration of the initial condition setup for a two dimensional detonation wave (Lefebre, Oran & Kailansanath (1993)).

Expanding the $1D$ solution over a $2D$ domain and adding an unreacted pocket results in the initial conditions shown in Fig. 2.4.

One additional feature of the initial conditions is that the velocity in the direction of the detonation wave was subtracted by DCJ. This makes the detonation propagate in way that is stationary with respect to the computational domain, allowing for the physics to be captured in a smaller computational domain and, as a result, reduces the computational

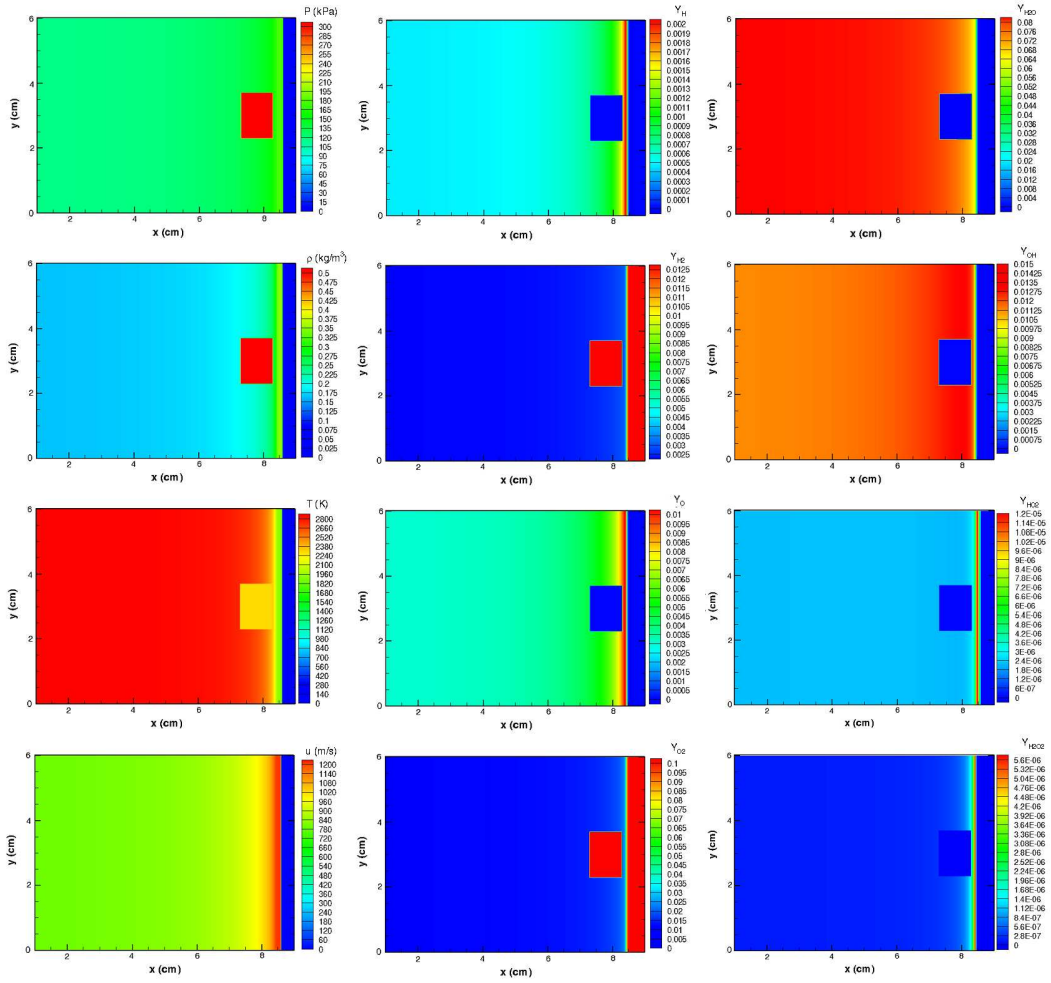

Figure 2.4: Contour plots of the initial thermodynamic properties and species concentrations.

expense of the simulation.

2.3 Boundary Conditions

The boundary conditions used for the inviscid detonation simulation were reflective for the top and bottom walls.

$$\mathbf{u} \cdot (\mathbf{n}) = \mathbf{0} \tag{2.12}$$

The side walls are outflows that are represented by Dirichlet boundary conditions.

$$\frac{\partial \mathbf{q}}{\partial \mathbf{n}} = 0 \tag{2.13}$$

Where $\mathbf{q} = [\rho_1, ..., \rho_s, \rho u, \rho v, \rho E]$

Chapter 3

NUMERICAL METHODS

3.1 Numerical Scheme

The numerical scheme used in this simulation was a WENO scheme proposed by Hill & Pullin (2004). Initially, the flux is split into two parts, one part that is strictly negative and one that is strictly positive: $f(x) = f^+(x) + f^-(x)$. The splitting was done using a Roe averaged Jacobian decomposition. The procedure for computing the derivative at the jth is to first interpolate flux values on the half grid points $f_{j-1/2}$ and $f_{j+1/2}$ and then form the difference

$$\frac{df}{dx} = \frac{1}{\Delta x}\left(f_{j+1/2} - f_{j-1/2}\right) \tag{3.1}$$

The interpolated values are the weighted sum of the individual interpolations $q_k|_{j+1/2}$. Each of these is produced by a candidate stencil $a_{k,l}$ and combined.

$$f_{j+1/2} = \sum_{k=0}^{3} \omega_k q_k \tag{3.2}$$

$$q_k|_{j+1/2} = \sum_{l=1}^{3} a_{k,l} f\left(x_{j-2+k+l}\right) \tag{3.3}$$

The weights α_k are defined as follows

$$\alpha_k = \frac{C_k}{(\epsilon + IS_k)^2} \tag{3.4}$$

and then normalized

$$\omega_k = \frac{\alpha_k}{\sum_{k=0}^{3} \alpha_k} \tag{3.5}$$

where ϵ exists to avoid divide by zero situations in the code.

The smoothness is defined as follows

$$IS_k = \sum_{m=1}^{2} \int_{x_{j-1/2}}^{x_{j+1/2}} (\Delta x)^{2m-1} \left(\frac{\partial^m q_k}{\partial x^m} \right)^2 dx \tag{3.6}$$

and can be computed using

$$IS_k = \sum_{m=1}^{2} \left(\sum_{l=1}^{2} d_{l,m,k} f\left(u_{j-1+l+k}\right) \right) \tag{3.7}$$

The WENO scheme was defined in a way that would allow integration with TCD at a later date to leave turbulence modeling in the detonation simulations open. The simulations conducted in this thesis used a pure WENO scheme.

$$\sum_{k=1}^{3} d_k \left(f\left(x_{j+k}\right) - f\left(x_{j-k}\right) \right) = \sum_{k=0}^{3} C_k \sum_{l=1}^{3} a_{k,l} \left(f\left(x_{j-2+k+l}\right) - f\left(x_{j-3+k+l}\right) \right) \tag{3.8}$$

Table 3.1 shows the interpolation superposition weights, Table 3.2 shows the stencil coefficients and Table 3.3 shows the stencil smoothness coefficients.

k	0	1	2	3
C_k	0.1815	0.31845	0.31845	0.1815

Table 3.1: The interpolation superposition weights of the numerical scheme.

.

k	$l=1$	$l=2$	$l=3$
$a_{k,l}$	.	.	.
0	$1/3$	$-7/6$	$11/6$
1	$-1/6$	$5/6$	$1/3$
2	$1/3$	$5/6$	$-1/6$
3	$11/6$	$-7/6$	$1/3$

Table 3.2: The stencil coefficients of the numerical scheme.

.

k	$l=1$	$l=2$	$l=3$
$d_{k,l}$	.	.	.
0	$1/2$	-2	$3/2$
1	$-1/2$	0	$1/2$
2	$3/2$	-2	$1/2$
3	$-5/2$	4	$-3/2$

Table 3.3: The stencil smoothness coefficients of the numerical scheme.

.

3.2 Adaptive Mesh Refinement

Due to the fact that, in detonation simulations, grid spacing requirements have high spatial and temporal variance, it is necessary, for computational efficiency, to refine different regions of the grid differently. This is accomplished through the use of an adaptive mesh refinement algorithm (Berger & Colella (1989)).

This method works by distributing nested grids inside of the main grid, and if necessary, grids inside of those. The nested grids are then iterated in between the time steps of the main grid to achieve higher resolution where they exist.

An algorithm for accomplishing this is as follows.

$$G_l = \bigcup_k G_{l,k} \tag{3.9}$$

This is illustrated in Fig. 3.1.

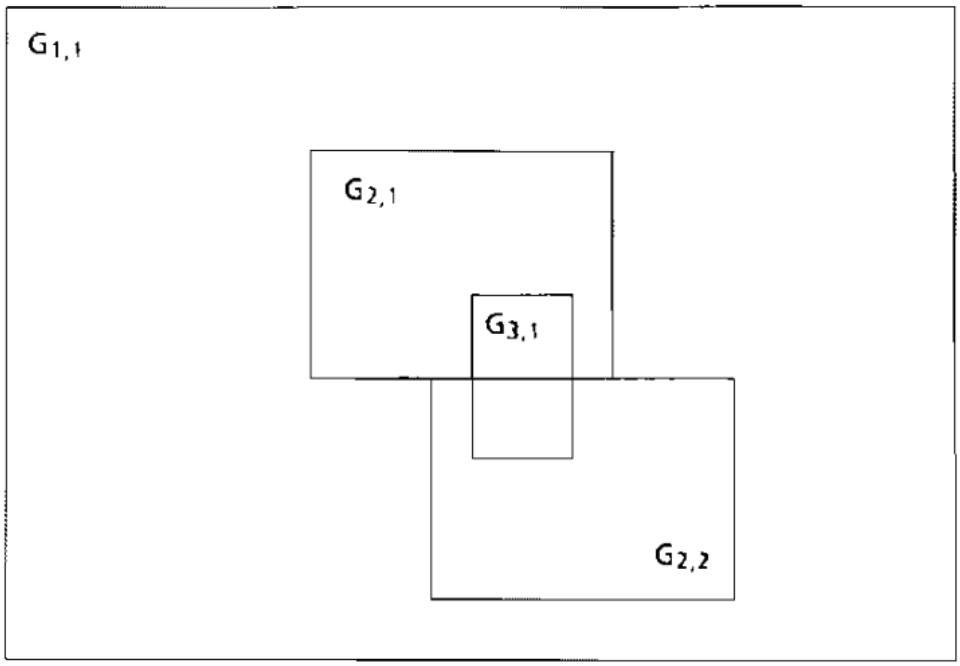

Figure 3.1: Illustration of the nested grids concept used for adaptive mesh refinement (Berger & Colella (1989))

1. A fine grid starts and ends at the corner of a cell in the next coarser grid

2. There must be at least one level $l-1$ cell in some $l-1$ grid separating a grid cell at level l from a cell at level $l-2$, in the north, south, east, and west directions, unless the cell abuts the the physical boundary of the domain.

Grids are refined in time as well as space by the refinement ratio r where

$$r = \frac{\Delta_{l-1}}{\Delta_l} \tag{3.10}$$

$$\frac{\Delta t_l}{\Delta x_l} = \frac{\Delta t_{l-1}}{\Delta x_{l-1}} = ... = \frac{\Delta t_1}{\Delta x_1}. \tag{3.11}$$

When coarser grids than the finest grids are iterated upon, the finer cells within it must be averaged. This is expressed as

$$u_{l,j}^{coarse} \leftarrow \frac{1}{r^2} \sum_{p=0}^{r-1} \sum_{q=0}^{r-1} u_{k+p,m+q}^{fine} \tag{3.12}$$

Whenever an adjacent cell has finer resolution than the cells around it, the flux is averaged on that cell as part of the iteration procedure.

3.3 Parallelization

The code was run on multiple processors, and to operate effectively, it was necessary to use an algorithm to distribute the workload in an efficient way. The process by which this is done is simple for the case of a uniform mesh. However, with an adaptive mesh, it becomes much more complicated given that the distribution, concentration and number of grid points are not known a priori.

An effective tool for distributing processor work for this kind of problem is the Hilbert space filling curve. An illustration of this is shown in Fig. 3.2.

The line drawn through the mesh can be used to distribute processors in a simple, linear fashion in a way that makes signal passing between the processors efficient.

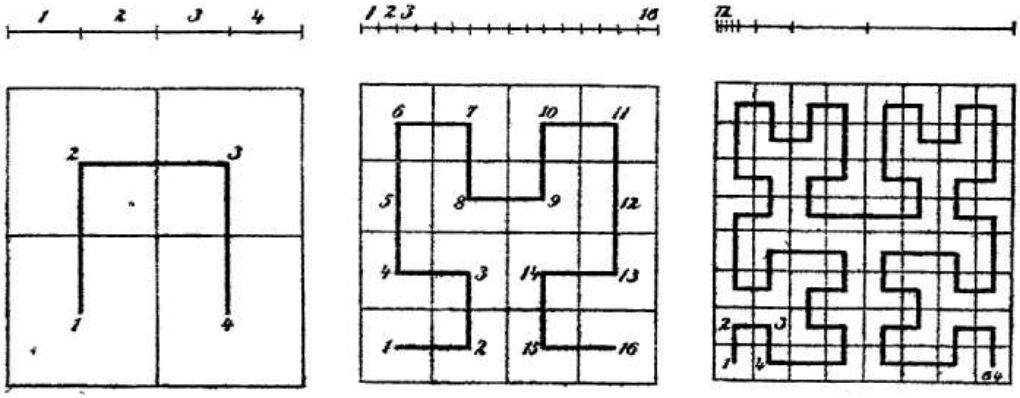

Figure 3.2: An illustration of the Hilbert space filling curve (Hilbert (1891)).

3.4 Lengthscale Determination

Once the methods have been defined, it is important to also define the scale at which the physics should be resolved. The component of a detonation that requires the highest precision is the flamelet directly behind the detonation in the region with maximum thermicity. An equation exists to calculate the flamelet lengthscale that is shown in Eq. 13.3. (Radulescu et al (2007)).

$$l_{diff} = \sqrt{\kappa t_{chem}} \tag{3.13}$$

Using this formula, the experimental data of Pintgen et. al (Pintgen et al (2003)) and the CEA code (Gordon & McBride (1994)) to determine the thermal diffusion behind the wave, the flamelet lengthscale was determined to be $6\mu m$.

In order to adhere to this requirement, the mesh parameters in Table 3.4 were chosen.

AMR Levels	r_1	r_2	r_3	L_x	L_y	N_x	N_y
3	4	4	4	10cm	6cm	100	40

Table 3.4: Mesh parameters used in the simulation.

These parameters result in the maximum mesh resolutions shown in Table 3.5.

Δx	Δy
$15.6\mu m$	$23.4\mu m$

Table 3.5: Maximum mesh resolution used in the simulation

The smallest lengthscales were chosen to be equal to 2-3 flamelet lengths in the direction of propogation. The most computationally intensive part of the simulation is the triple point, for which an approximate lengthscale calculation is difficult to make.

Because the thermodynamic property and species gradients are higher in the direction of the detonation's propagation than in the direction orthogonal to it's motion, it is assumed that it is acceptable to use a larger cell length orthogonal to th detonation's propagation, hence Δy being greater than Δx. The time step was chosen to be dictated by a CFL number of 0.1.

Chapter 4

RESULTS

4.1 Two Dimensional Cellular Detonation

The results of the simulation at a time of $17\mu s$ are shown in Fig. 4.1. What is shown in Fig. 4.1 is the beginning of the periodic asymmetry in the detonation front. The higher pressure near the center of the detonation wave due to the energy release of the reaction of the pocket behind it causes the center of the wave to, initially, move faster than the other regions of the detonation wave. The asymmetry of velocities along the length of the detonation wave caused by the disturbance causes the detonation wave to become locally curved. The unreacted gas, then, due to the curvature of the detonation front, moves through the detonation wave at a non-zero angle relative to the wave's propagation. This causes there to be a transverse propagation by the curved part of the detonation wave. As the curved part of the detonation wave moves outward, a local region of high vorticity forms at the interface between the directly propagating region of the detonation and region of the detonation containing a transverse disturbance. Due to the high temperature of this region, the reaction rate increased beyond the capabilities of the methods used to analyze this phenomenon after $t = 17\mu s$.

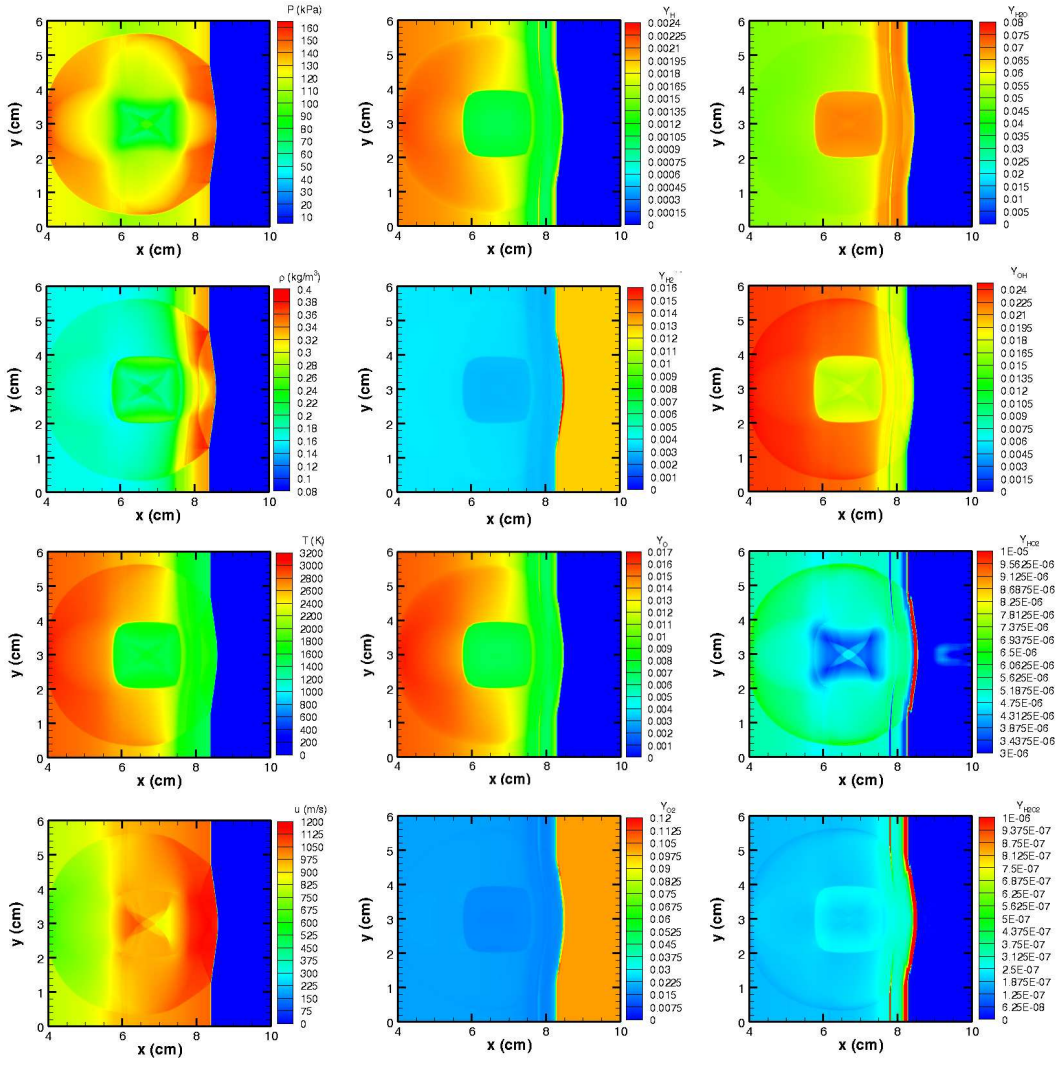

Figure 4.1: Contour plots of the thermodynamic properties and species concentrations at $t = 17\mu s$

Chapter 5

SUMMARY

This study was concerned with the simulation of detonation waves using a weighted essentially non-oscillatory scheme. The main objective was to develop a code that could be used to better understand the physics of detonation, which is necessary to develop controllable detonation waves for use in detonative propulsion. First, a 1D simulation was performed using ZND theory and the Hydrogen-Oxygen mechanism developed by Williams. This solution was then extrapolated across a two dimensional domain with a disturbance containing unreacted gases superimposed on top of it. From this starting point, the simulation was evolved on an adaptive mesh using a 2nd order weighted essentially non-oscillatory scheme with the smallest length scales chosen to be equal to approximately two flamelet lengths.

The results of the 1D simulation used to develop the initial conditions of the 2D simulation was successful. The 2D simulation, matched the qualitative structure of a detonation wave, however the simulation did not last long before crashing. The end of the simulation coincided directly with the formation of the triple point, which has the highest temperature, and thus the highest reaction rate, of any point in the detonation wave. Future simulations may be more successful if the grid is refined further so that more than one grid point exists in the flame, via a more efficient AMR code or if the weighted essentially non-oscillatory numerical scheme is changed to one that is higher order.

BIBLIOGRAPHY

Berger, M. J. and Colella, P. 1989 Local Adaptive Mesh Refinement for Shock Hydrodynamics **82** 64–84 *Journal of Computational Physics*

Bone, W. A., Fraser, R. P. and Wheeler, W. H. 1935 The Detonation Process in Gases. *Philosophical Transactions of the Royal Society* **35**, 235:29.

Chapman, D. 1889 . *Phil. Mag* pp. 47:90–104.

Deiterding, R. 2002 Efficient Simulation of Multi-Dimensional Detonation Phenomena *ALGORITHMY Conference on Scientific Computing.*

Döring, W. 1943 The Detonation Process in Gases. *Ann. Phys.* **43**, 421–436.

Gordon, S. and McBride, B. J. 1994 Computer Program for Calculation of Complex Chemical Equilibrium Compositions and Applications **1311** *NASA Report*

Hilbert, D. 1891 Ueber die stetige Abbildung einer Linie auf ein Flachenstuck. *Math. Ann.*

Hill, D. J. and Pullin, D. I. 2004 Hybrid Tuned Center-Difference-WENO Method for Large Eddy Simulations in the Presence of Strong Shocks **194** 435–450 *Journal of Computational Physics*

Jouguet, J. C. E. 1904 Sur londe Explosive. *CR Acad. Sci. Paris* **139**, 121–124.

Lee, J. H. S. 2008 The Detonation Phenomenon

Lefebre, M. H., Oran E. S. and Kailansanath, K. 1993 The Influence of Heat Capacity and Diluent on Detonation Structure **95** 206–218 *Combustion and Flame*

Pintgen, F., Eckett, C. A., Austin, J. M. and Shepherd, J. E. 2003 Direct Observations of the Reaction Zone Structures in Propagating Detonations **133** *Combustion and Flame*

Lee, J. H. S. and Radulescu, M. I. 2005 On the Hydrodynamic Thickness of Cellular Detonations **41** 745–765 *Annual Review of Fluid Mechanics*

Radulescu, M. I., Sharpe, G. J., Chung K. L. and Lee, J. H. S. 2007 The Hydrodynamic Structure of Unstable Cellular Detonations. **580***Journal of Fluid Mechanics*

Zeldovich, Y. B. and Ratner, S.B. 1941 *ZhETF* **1** 11:170

Robert, J. 1989 Chemkin-II: A Fortran Chemical Kinetics Package for the Analysis of Gas-Phase Chemical Kinetics *Sandia National Laboratories Report*

Kao, S. and Shepherd, J. E. 2008 Numerical Solution Methods for Control Volume Explosions and ZND Detonation Structure `www2.galcit.caltech.edu/EDL/public/cantera/doc/text/CVZND/CVZND.pdf`

von Neumann, J. 1942 Theory of Detonation Waves. Rep. 549. O.S.R.D.

Williams, F. A. 1985 Combustion Theory *Perseus Books Publishing.*

Williams, F. A. 2004 Descripions of Hydrogen-Oxygen Chemical Kinetics for Chemical Propulsion. *International Symposium on Energy Conversion Fundamentals*

Zeldovich, Y. B. 1940 The Question about Energetic Use of Detonation combustion. *Zh. Tech. Fiz,* **10**, 1453–1461.